Published by :
https://www.ijert.org/
An International Peer-Reviewed Journal

International Journal of Engineering Research & Technology (IJERT)
ISSN: 2278-0181
Vol. 15 Issue 04 , April - 2026

# Computational Study of Laminar and Turbulent Shock Wave Boundary Layer Interactions at Mach 5

Nishma K B and Jayahar Sivasubramanian
Department of Aerospace and Automotive Engineering
M. S. Ramaiah University of Applied Sciences
Bangalore, India

***Abstract*** **- Shock wave boundary layer interaction (SWBLI) is a key phenomenon in high-speed aerodynamics, influencing aerodynamic efficiency, stability, and thermal loading. This study employs the SU2 solver to investigate SWBLI in laminar and turbulent regimes. Initially, two-dimensional turbulent cases for three different wedge angles are validated against experimental data to ensure numerical accuracy. The analysis then focuses on laminar interactions, where low-momentum boundary layers are more susceptible to shock-induced adverse pressure gradients, leading to flow separation, recirculation bubbles, and delayed recovery. Reynolds number effects are examined by systematically reducing freestream pressure, thereby altering both shock strength and viscous properties. Results indicate that lower Reynolds numbers generate weaker shocks and shorter separation bubbles with earlier reattachment, whereas higher Reynolds numbers produce stronger shocks, longer bubbles, and delayed reattachment despite higher boundary layer resistance. The study highlights the coupled influence of Reynolds number and freestream conditions on laminar SWBLI, providing insights that enhance predictive capability for high-speed vehicle design and optimization.**

***Keywords – SWBLI, Laminar, Turbulent, Separation Bubble***

## I. INTRODUCTION

Shock wave boundary layer interaction (SWBLI) is a critical phenomenon encountered in high-speed flows, particularly in supersonic and hypersonic regimes. When a shock wave interacts with the boundary layer developing over a surface, it imposes an adverse pressure gradient, which can lead to complex flow behaviors such as boundary layer separation, formation of recirculation bubbles, and the generation of secondary shock structures. These interactions significantly affect the aerodynamic performance, stability, and thermal loads on aerospace vehicles, with practical implications ranging from air intake design to thermal protection systems [1][2].

The behavior of the boundary layer under such interactions is strongly dependent on whether it is laminar or turbulent. Despite the extensive research in SWBLI, much of the existing knowledge is based on experimental observations or simplified models. There remains a need for detailed computational studies to capture the intricate physics of both laminar, turbulent and transitional interactions under various flow conditions. A computational approach enables precise control of flow parameters, shock strengths, and boundary layer properties, facilitating a deeper understanding of the interaction mechanisms. Therefore, the motivation behind this research is to conduct a comprehensive computational study of laminar, turbulent shock boundary layer interactions, focusing on the key flow features such as separation, reattachment, recirculation bubbles, shock reflection patterns, and their impact on aerodynamic characteristics.

To ensure accuracy, the study begins with validating turbulent 2D simulations against experimental data using the SU2 solver. After validation, laminar cases are examined to understand how the nature of the boundary layer affects interaction strength, separation, and pressure distribution. In the present study, a computational investigation of shock wave Laminar and turbulent boundary layer interaction is carried out using the open-source CFD solver SU2**.** The configuration involves an oblique shock generated by a wedge impinging on a flat plate, representing a canonical SWBLI case. Three wedge angles 6°, 10°, and 14° are considered to examine their influence on surface pressure, skin friction, and heat flux distributions. The numerical results are validated against the experimental data of [13] to assess the predictive capability of turbulence models in SU2. This study underscores the limitations of existing models in capturing shock-induced separation and highlights the need for accurate numerical modelling in high-speed aerodynamic design.

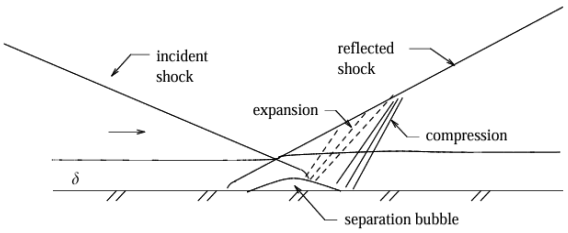


Fig.1 Shock Wave Boundary Layer Interaction [2]

## II. LITERATURE REVIEW

Laminar SWBLI, though less explored compared to its turbulent counterpart, is highly relevant in low Reynolds number environments such as high-altitude flight and early atmospheric re-entry. Laminar boundary layers possess lower near-wall momentum and are therefore more susceptible to adverse pressure gradient–induced separation, often leading to earlier separation onset, larger relative separation bubbles, and stronger localized heat-flux amplification for a given shock

International Journal of Engineering Research & Technology (IJERT)
ISSN: 2278-0181
Vol. 15 Issue 04 , April - 2026

strength. In [4] the authors numerically examined the interaction between an oblique shock and a laminar boundary layer under hypersonic flow conditions, showing that shock impingement significantly influences separation, reattachment, and surface pressure and heat transfer distributions. Similarly, [3] demonstrated that variations in shock strength and geometry can trigger or accelerate transition and strongly affect heat-flux levels. These works collectively highlight that laminar SWBLI behavior is highly dependent on Reynolds number, which controls boundary-layer thickness, viscous diffusion, and near-wall momentum. Additionally, freestream pressure and temperature variations alter both shock strength and viscous effects, leading to complex coupled behavior between shock dynamics and boundary-layer response. Despite qualitative understanding from existing numerical and experimental studies, quantitative prediction of laminar separation, transition onset, and associated thermal loads remains limited, emphasizing the need for advanced high-fidelity simulations and improved diagnostic techniques for accurate modeling of aerodynamic and thermal responses in laminar-dominated hypersonic flows.

Turbulent SWBLI has been extensively investigated due to its critical role in high-speed aerodynamics, where accurate prediction of pressure loads, heat transfer, and flow separation is essential for vehicle design and thermal protection. In turbulent boundary layers, the higher near-wall momentum provides greater resistance to shock-induced separation; however, strong shocks can still cause significant separation zones, delay pressure recovery, and amplify surface heat flux. Reference [11] highlight that, despite major advancements in computational methods and experimental diagnostics, accurate prediction of unsteady pressure loads, heat flux peaks, and three-dimensional effects remains limited. Similarly, [13] revealed that existing turbulence models often assume a direct analogy between momentum and heat transfer, which fails to capture their distinct behavior under strong interaction conditions. Further investigations demonstrated that current Reynolds-Averaged Navier–Stokes (RANS) models, including the Menter Shear Stress Transport (SST) model, tend to underpredict separation extent and heat-flux amplification in strong interactions. These studies collectively indicate that while turbulent SWBLI is relatively well-characterized compared to laminar cases, challenges persist in accurately modeling unsteady, three-dimensional, and high-enthalpy effects, underscoring the need for improved turbulence and transition modeling coupled with high-fidelity simulations.

## III. METHODOLOGY

In the present investigation, the shock wave boundary layer interaction is being studied as an internal flow between the shock generator and the flat plate. Thus, three different angles are considered for the study: $6^0$, $10^0$ and $14^0$. According to the experiments, the inviscid shock is impinging at the location of 350mm from the leading edge of the flat plate. Thus, all the three geometries are designed so that the shock impinges at the same location on the flat plate as given in the experiment. This helps in validating the surface parameters results obtained. The shock generator length is of 300mm as stated in the experiments. The flat plate length is considered to be of 1000mm. The distance between the flat plate and the shock generator is fixed as 125mm (see (2)) [13]. All the geometry points are taken directly into the commercially available meshing software and geometry was created and meshed.

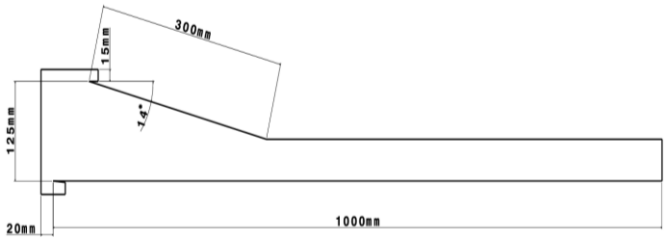


Fig. 2 Geometry of the SWBLI configuration with dimensions.

The computational domain extends from (-10, 1000) mm in x direction, the initial domain is extended to initialize the flow before the flow hits the compression corner or the shock generator. Meshes of three different grid sizes were generated, coarse, medium and fine mesh. The domain consists of boundary layer attached along the entire wall region, i.e., wedge and the flat plate respectively (as in (3)). $y^+$ of 1 is considered for the creation of the boundary layer, with the first layer spacing of 0.001 mm. In all the computations, the mesh was kept finer near the wall region and the separation region (3). The mesh is made coarser away from the interaction region. The region away from the interaction region is made to capture the reflected shock from the separation bubble and the expansion fans from the trailing edge of the wedge or shock generator.

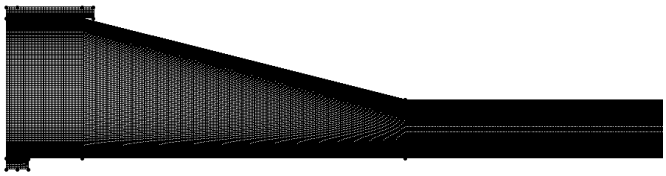

Fig. 3 Representation of the grid in the computational domain.

Table 1. Flow Properties for Laminar Cases

| M | $P_\infty$ | $T_\infty$ | Re |
|---|---|---|---|
| 5 | 500 Pa | 970K | 155000/m |
| 5 | 650 Pa | 975K | 199000/m |
| 5 | 990 Pa | 1160K | 224000/m |

**Table 2.** Boundary Conditions for Turbulent Cases

| Boundary Conditions | Boundary Definitions |
|---|---|
| Flat plate , Wedge | Wall- No slip |
| Inlet | Pressure Farfield |
| Outlet | Pressure outlet |

**Table 3.** Freestream Flow Properties for Turbulent Cases

| M | $P_\infty$ | $T_\infty$ | Re |
|---|---|---|---|
| 5 | 4006.8636 Pa | 68.33K | $37\times10^6$/m |

For the current investigation, the open-source SU2 solver [8], developed at Stanford University, is employed. SU2 is based on the finite volume method and is capable of solving complex compressible flows. In the turbulent cases, the governing equations are the Reynolds-averaged Navier Stokes (RANS) equations, with Menter's Shear Stress Transport (SST) model selected for turbulence closure. Venkatakrishnan's

International Journal of Engineering Research & Technology (IJERT)
ISSN: 2278-0181
Vol. 15 Issue 04 , April - 2026

second-order flow limiter is implemented to enhance convergence stability, while an adaptive CFL strategy is applied, with values ranging from 0.1 to 4, to accelerate solution convergence. The viscosity variation with temperature is modelled using Sutherland's law, ensuring physically accurate representation of high-speed viscous effects. For convective flux calculations, the Harten Lax van Leer Contact (HLLC) scheme is chosen. This scheme is a second-order approximate Riemann solver widely used for hyperbolic systems, particularly effective in capturing discontinuities such as shock waves. Post-processing of the numerical results is carried out using Paraview for visualizing flow field contours such as Mach number, Wall pressure, and Skin Friction distributions and heat flux distributions. Tec plot is employed for comparative data analysis between computational predictions and available experimental results [11,12].

## IV. RESULTS AND DISCUSSION

### *A. Laminar SWBLI*

Laminar SWBLI is a key phenomenon in hypersonic aerodynamics, especially in low Reynolds number environments such as high-altitude flight and early atmospheric reentry. In these conditions, the flow remains laminar over extended surface regions, making the study of laminar SWBLI critical for accurate prediction of surface loads on hypersonic vehicles. When a shock wave impinges on a laminar boundary layer, it creates an adverse pressure gradient, which can lead to boundary layer separation. The resulting separation bubble and reattachment significantly affect surface properties. Reynolds number plays a central role in determining the extent of this interaction. A lower Reynolds number generally leads to weaker wall shear, larger separation zones, and delayed reattachment. Surface pressure, skin friction, and heat flux distributions are all highly sensitive to Reynolds number variations in laminar SWBLI. Understanding this sensitivity is necessary for precise aerodynamic and thermal load predictions. When an oblique/normal shock meets a laminar boundary layer the inviscid flow outside the BL jumps to a higher static pressure. That produces a strong adverse pressure gradient (APG) felt at the wall. A laminar BL has low momentum near the wall (small wall shear) compared with a turbulent BL, so it cannot resist the APG as the near-wall velocity profile decelerates, the wall shear falls to zero, flow reverses and a separation bubble forms upstream of the shock; downstream you get reattachment and a thin recovery region. Laminar interactions therefore tend to have earlier separation, larger separation bubbles (relative to BL thickness), and stronger local heat-flux amplification than turbulent interactions for the same shock strength. A baseline laminar case is first considered, and the flow is maintained in the laminar regime throughout the interaction region. To examine the influence of Reynolds number, the freestream temperature and pressure are systematically reduced, thereby lowering the Reynolds number while keeping other parameters constant. This approach allows the observation of changes in separation bubble size, surface pressure distribution, and skin friction at lower Reynolds numbers. The results provide insights into the sensitivity of laminar SWBLI to variations in freestream conditions and highlight the differences in flow behavior compared to turbulent SWBLI [2][3].

***6° wedge case***

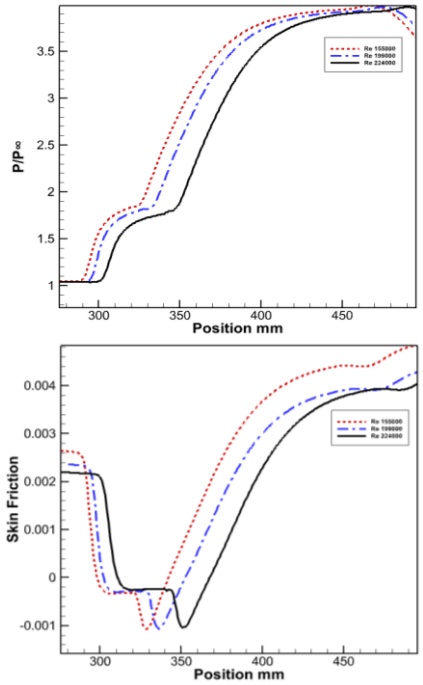


Fig. 4 Pressure Distributions and Skin Friction Distributions.

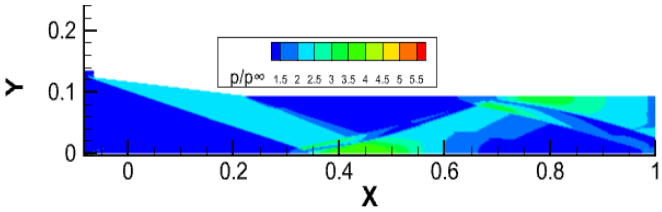


Fig. 5 Pressure Contour.

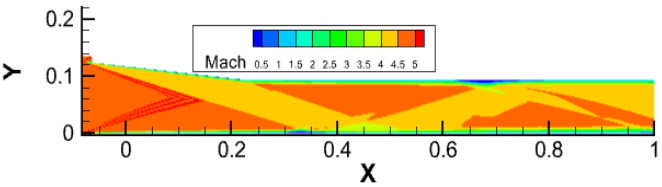


Figure.6 Mach Number Contour.

Fig. 4 shows the normalized wall pressure (p/p∞) distribution along a flat plate for Reynolds numbers 150,000, 190,000, and 224,000 at a 6° wedge. Up to 300 mm, p/p∞ ≈ 1 indicates undisturbed laminar flow. Around 300 mm, a sharp pressure rise marks the impinging oblique shock, followed by a plateau representing the separation bubble. A second rise denotes reattachment and the reattachment shock, after which pressure stabilizes as the flow reattaches. Reynolds number was varied by reducing freestream pressure and temperature, which decreased density, viscosity, and dynamic pressure. At lower Re, the weaker shock produces a smaller or earlier-reattaching separation bubble, leading to earlier pressure recovery. Although low Re usually delays reattachment, the weaker shock offsets this effect, showing that SBLI behavior depends on both Re and shock strength. Without a shock, lower pressure reduces density and Re, weakening near-wall momentum so that adverse pressure gradients cause earlier

International Journal of Engineering Research & Technology (IJERT)
ISSN: 2278-0181
Vol. 15 Issue 04 , April - 2026

and more extensive separation typical of laminar flow. In contrast, when a shock is present, the sudden pressure rise can cause separation if the boundary layer lacks sufficient momentum to resist it. The separation bubble length is thus governed by two competing factors: shock strength, which increases separation, and boundary-layer momentum, which resists it.

When the freestream static pressure P∞ decreases, the total pressure of the flow is reduced (see Fig. 5). For the same Mach number, this leads to a lower absolute dynamic pressure. A lower dynamic pressure means that the shock produces a smaller absolute pressure rise across it (in pascals), even though the pressure ratio may remain similar. With a weaker shock, the adverse pressure gradient is reduced, which in turn tends to shrink the separation bubble.

Fig. 5 shows that the skin-friction coefficient ($C_f$) drops sharply at the shock impingement due to the adverse pressure gradient, with negative value indicating reversed flow. Reattachment occurs when $C_f$ becomes positive again. At low Re (155,000), the thicker, weaker boundary layer produces a deeper negative $C_f$ but reattaches sooner. At high Re (224,000), the thinner, stronger boundary layer shows a smaller dip yet reattaches later, giving a longer separation. Thus, lower Re causes stronger reversal but shorter separation. When the Reynolds number is low, viscous forces dominate over inertial forces. In practical terms such as when the freestream static pressure $p_\infty$ is reduced at the same Mach number several things conspire to push Re down, such as the density $\rho_\infty$ drops strongly, the speed $U_\infty$ also drops. The net effect is a lower Re. A lower Reynolds number reshapes the boundary layer by making viscous diffusion relatively stronger, leading to a thicker layer with weaker near wall inertia. As a result, low-Re laminar boundary layers are highly sensitive to shocks and reach separation criteria more readily, even under weaker forcing. In shock–boundary layer interactions, this means separation can occur abruptly at low Re, with distinct differences from high-Re cases. Lower $p_\infty$ reduce the absolute dynamic pressure $q_\infty$, so for the same Mach number the shock's absolute pressure jump (in pascals) is weaker. The weaker shock forcing tends to shorten the overall separation bubble. However, the thicker, low-Re laminar boundary layer is more susceptible to reverse flow once separation begins, leading to stronger local recirculation relative to the weakened freestream momentum. As a result, these effects can coexist and the bubble may be shorter overall, yet the internal reversal can be more intense, producing a deeper negative dip in the skin-friction coefficient before the reattachment spike [4].

### *10° wedge case*

Fig. 7 shows normalized wall pressure (P/p∞) and skin friction coefficient ($C_f$) along a flat plate for three laminar Reynolds numbers (155,000, 199,000 and 224,000) at the same Mach number. Upstream (x < 300 mm), P/P∞ ≈ 1 and $C_f$ > 0, indicating an attached laminar boundary layer. The 10° wedge generates a stronger oblique shock than the 6° case, producing a larger initial pressure rise and stronger adverse pressure gradient. The Adverse pressure gradient thickens and decelerates the boundary layer, leading to separation. The first pressure rise corresponds to the incident shock, while the larger downstream rise marks reattachment and recompression. Reynolds number strongly influences the interaction that is at low Re, weaker shock forcing and stronger viscous diffusion shorten the separation length and promote earlier pressure recovery. At high Re, the thinner, less diffusive boundary layer allows the APG to penetrate more deeply, producing stronger reversal that is larger negative skin friction (see (8)), a longer separation length, delayed reattachment, and stretched pressure recovery. Changes in freestream pressure therefore affect not only Re but also shock strength, coupling viscous and inviscid effects.

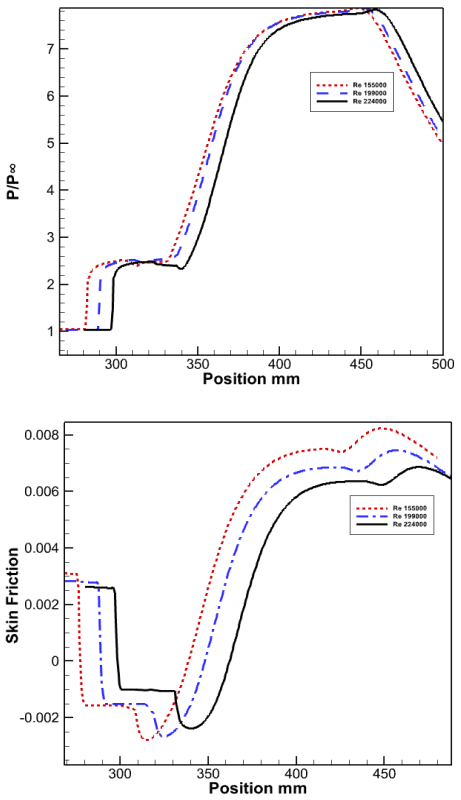


Fig. 7 Pressure Distributions and Skin Friction Distributions

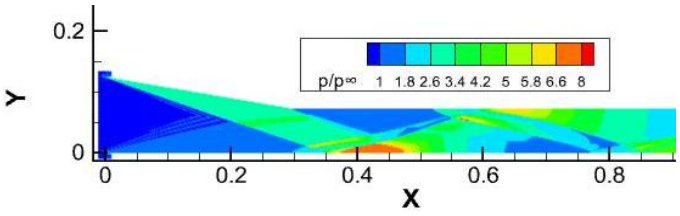


Figure.8 Pressure Contour

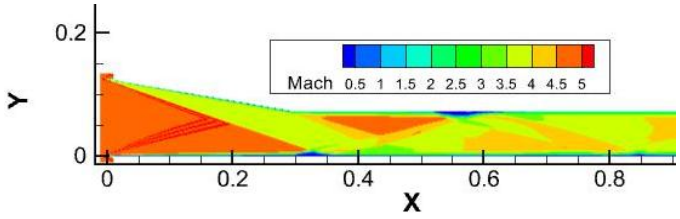


Figure.9 Mach Contour

International Journal of Engineering Research & Technology (IJERT)
ISSN: 2278-0181
Vol. 15 Issue 04 , April - 2026

***14° wedge case***

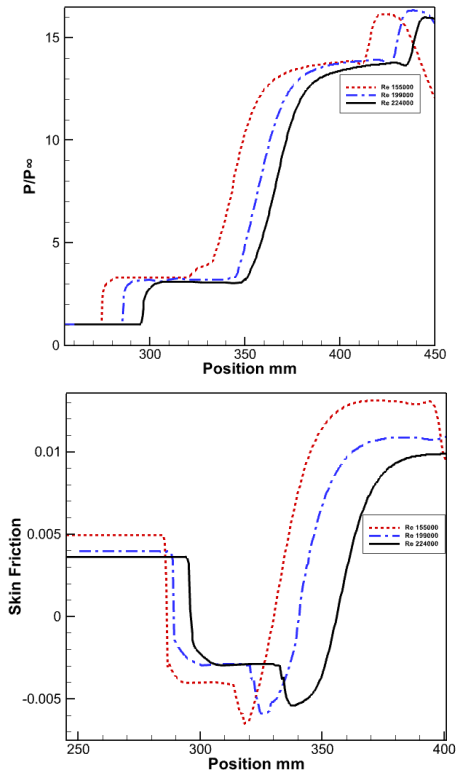


Figure.10 Pressure Distributions and Skin Friction Distributions

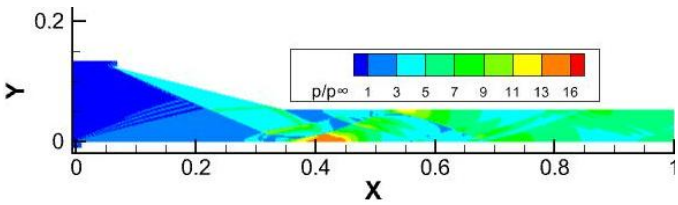


Figure.11 Pressure Contour

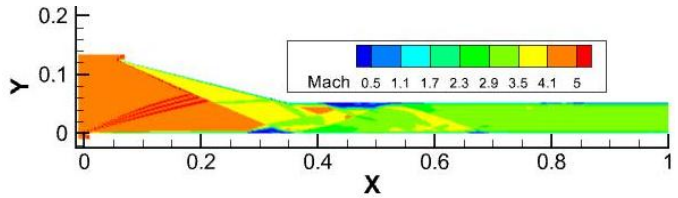


Figure.12 Mach Contour

For the 14° wedge case pressure plots (10) shows the strongest shock–boundary layer interaction, with the highest peak for pressure. Upstream of 300 mm, P/P∞ ≈1, indicating attached laminar flow. Shock impingement produces a sharp pressure rise, followed by a short plateau from the separation bubble, and a steep reattachment rise leading to a post-shock equilibrium of P/P∞ ≈13–14. In fig. 10 it is seen that $C_f$ is positive and constant upstream, drops sharply under the adverse pressure gradient, becomes negative in the separation bubble, and recovers to positive values after reattachment. The lowest Re case (155,000) shows the deepest negative $C_f$, but the shortest separation length due to weaker shocks. At higher Re (224,000), the thinner boundary layer resists separation initially, but stronger shocks delay reattachment, producing the longest bubble. Thus, separation length depends not only on Re but also on coupled freestream conditions that affect shock strength. Among all wedge angles, the 14° case produces the deepest $C_f$ trough and longest separation region, confirming it as the strongest interaction [3] [4].

*B. Turbulent SWBLI*

In hypersonic flow, shock wave turbulent boundary layer interactions play a critical role in determining surface pressure, wall shear stress, and overall aerodynamic performance. In a turbulent boundary layer, enhanced momentum exchange allows the flow to better resist separation under moderate adverse pressure gradients; however, when an impinging shock is sufficiently strong, separation still occurs, forming recirculation bubbles and complex shock systems. The turbulent nature of the boundary layer leads to increased mixing and energy dissipation, influencing both the size of the separation region and the reattachment characteristics [6]. Three different types of grids were considered for the study. The coarse mesh has cell size of 2,06,012, the medium mesh has cell size of 4,04,498, and the fine mesh has cell size of 6,18,122.

***6° Shock generator case ($\theta_w$ = 6°)***

As seen in Fig. 13 and Fig. 14, for 6° wedge case, it is observed that the shock wave generated from the wedge impinges on the flat plate, producing an adverse pressure gradient that acts opposite to the flow direction. This pressure rise pushes against the boundary layer and slightly lifts it away from the surface. However, the turbulent boundary layer has sufficient momentum to resist the pressure forces, so the flow does not fully detach from the wall. As a result, no separation bubble is formed, indicating that the interaction remains weak. At the point where the shock hits the plate, the boundary layer becomes thinner because of the local compression caused by the shock. This thinning of boundary layer supports the formation of the reflected shock from the flat plate. Downstream of the wedge, the flow expands as it turns outward, forming an expansion fan at the trailing edge. The expansion waves interact with the reflected shock further downstream, but since the reflected shock is weak, this interaction is smooth and does not significantly disturb the overall flow. The Mach contour (see Fig. 17) clearly shows a reduction in velocity at the shock impingement region, while the pressure and density contours (see Fig. 16 and Fig. 17) indicate an increase across the shock. The flow remains attached after the interaction, with no noticeable separation region or distortion. Hence, this case is characterized as a weak interaction where the boundary layer experiences only mild pressure effects and retains its stability throughout the flow field [9].

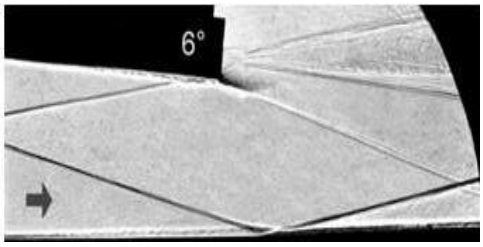


Figure.13 Experimental Shadowgraph for 6° wedge

International Journal of Engineering Research & Technology (IJERT)
ISSN: 2278-0181
Vol. 15 Issue 04 , April - 2026

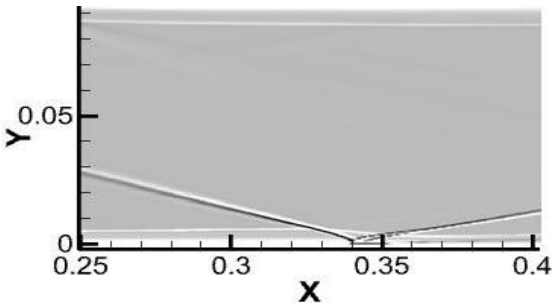


Figure.14 Computational Shadowgraph for 6° wedge case

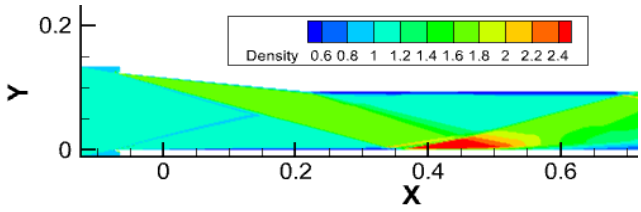


Figure.15 Density contour for 6° wedge case

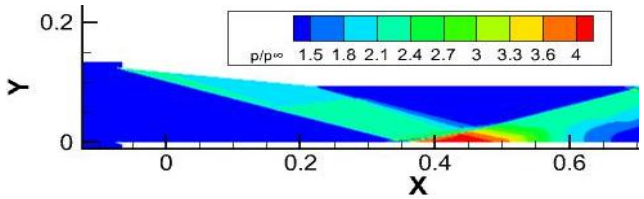


Figure.16 Pressure contour for 6° wedge case

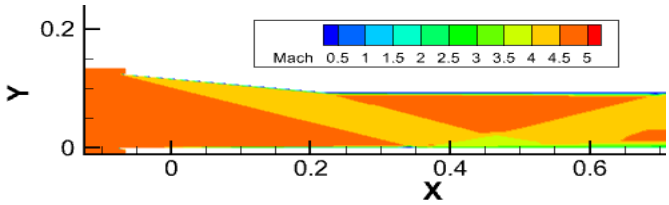


Figure.17 Mach contour for 6° wedge case

Since the 6° wedge case generates a weaker oblique shock the resulting interaction is characterised as weak shock boundary layer interaction, with minimal disruption to the boundary layer. The wall pressure rises moderately from approximately 4.1 kPa upstream to about 17 kPa (see Fig. 18 (a)). This behaviour reflects the limited shock strength associated with the small wedge angle. The SU2 simulation shows good agreement with experimental pressure data [7][9]. The skin friction coefficient drops to near zero at the separation point and becomes slightly negative within the separation bubble due to localized flow reversal. After reattachment, $C_f$ increases sharply, reaching a peak of 0.0029. While the separation location matches well between CFD and experiment, the reattachment $C_f$ shows a larger discrepancy, with an error of about 7.9 % (see Fig. 19 (b)). The negative value of $C_f$ is due to small amount of flow reversal. These minor deviations which are observed after reattachment, likely due to modelling assumptions such as turbulence model, grid resolution, or 2D assumption or experimental uncertainties. For the 6° wedge, when the shock impinges on the surface, the wall heat flux rises sharply due to the increased pressure and temperature gradients. In the separation region, even though skin friction drops to zero, the heat flux can still increase (see Fig. 18 (c)). This is because the shock interacting with the turbulent boundary layer enhances turbulence within the boundary layer and in the outer flow. The shock also compresses the flow, raising surface pressure and density, which together cause more heat transfer to the wall, even in the separated region.

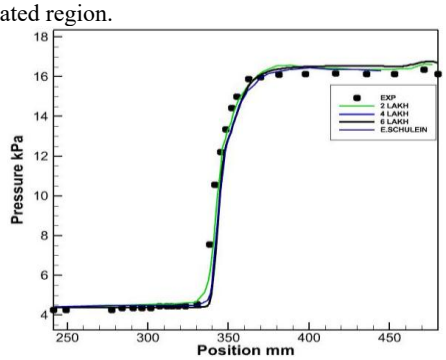


(a)

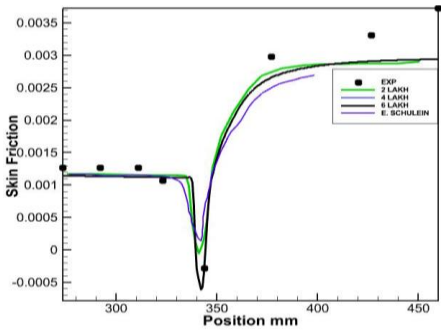


(b)

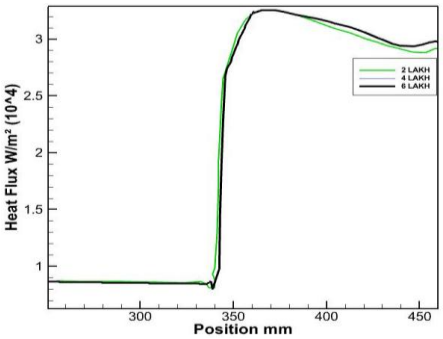


(c)

Fig. 18 (a) Surface pressure, (b) Skin Friction validation and (c) heat Flux Distributions for 6° wedge case

### *10° Shock generator case ( $\theta_w$ = 10°)*

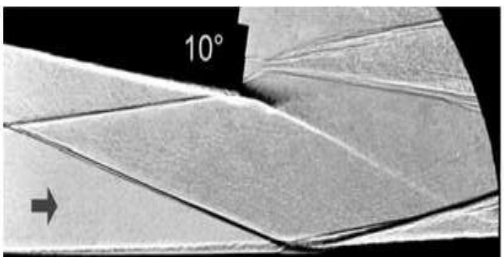


Fig. 19 Experimental shadowgraph for 10° wedge case.

International Journal of Engineering Research & Technology (IJERT)
ISSN: 2278-0181
Vol. 15 Issue 04 , April - 2026

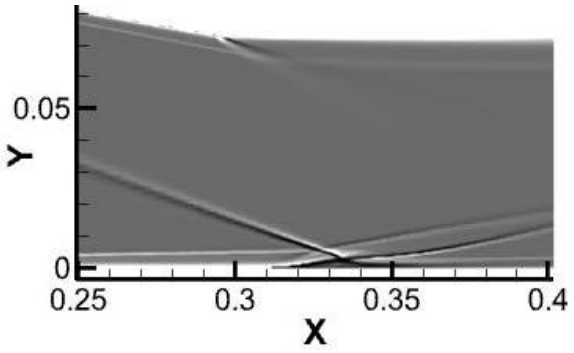


Figure.20 Computational shadowgraph for 10° wedge case

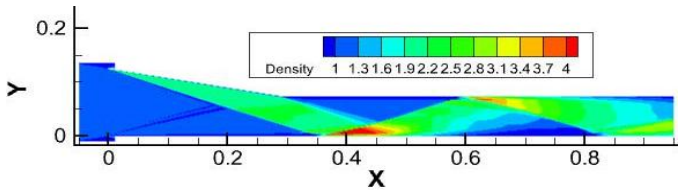


Figure.21 Pressure Contour for 10° wedge case

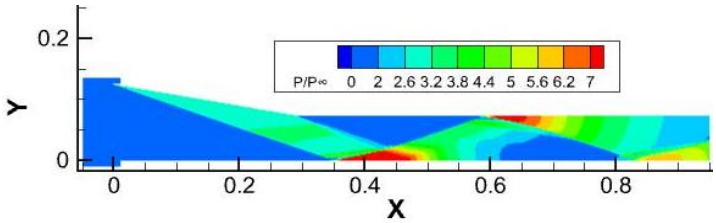


Figure.22 Pressure Contour for 10° wedge case

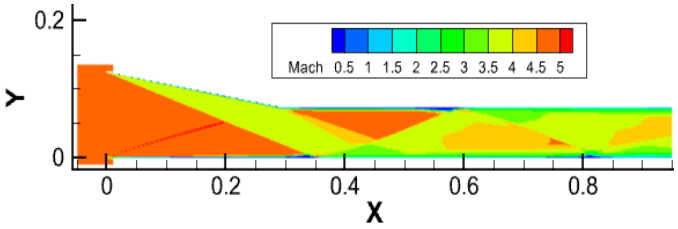


Figure.23 Pressure Contour for 10° wedge case

As seen from the contours in Fig. 19 and 20 a small but noticeable separation bubble forms for the 10° wedge case. The formation of this separation bubble causes the surface pressure to rise to a higher value compared to the 6° wedge case. This occurs because the separated flow reduces the ability of the boundary layer to follow the wall contour smoothly, causing a local buildup of pressure. The higher surface pressure in the separation region translates into increased pressure loads on the body. These higher pressure loads result in greater aerodynamic drag and energy loss, which ultimately reduces the overall performance and efficiency of the vehicle. In other words, the separation bubble not only alters the flow structure but also imposes additional forces that the vehicle must overcome, making it less efficient.

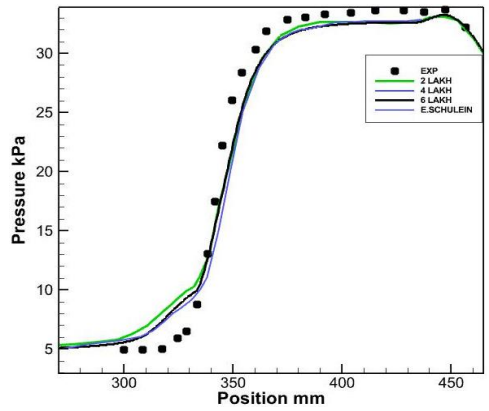


(a)

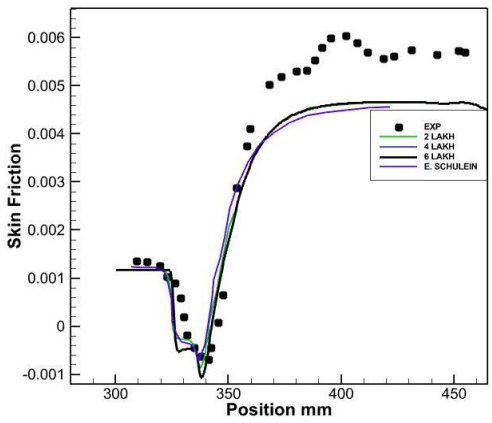


(b)

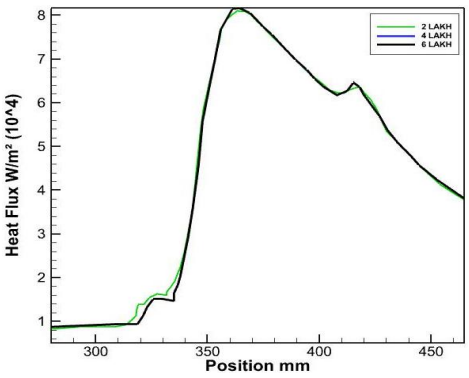


(c)

Figure.24 (a) Surface pressure, (b) Skin Friction validation and (c) heat Flux Distributions for 10° wedge case

The surface pressure rises from approximately 5 kPa to 33 kPa across the shock-impingement region, and the SU2 simulation closely matches the experimental surface-pressure data (see Fig. 24 (a)). This case represents a medium-strength shock-boundary layer interaction, and the RANS solver effectively captures the overall pressure rise. A small discrepancy at the reattachment point is observed, which can be attributed to complex flow structures and eddies within the separation bubble that locally increase the surface pressure and are challenging for steady RANS models to resolve accurately. The skin friction coefficient also shows good agreement with experimental data. The SU2 [12] simulation predicts a peak skin friction of $4.9\times10^{-3}$, whereas the

International Journal of Engineering Research & Technology (IJERT)
ISSN: 2278-0181
Vol. 15 Issue 04 , April - 2026

experimental peak is 6 $\times 10^{-3}$, resulting in a 7.9% error (see Fig. 24 (b)). The deviation occurs mainly post-reattachment, due to the limitations of the RANS approach in capturing highly turbulent and unsteady flows, the wall mesh resolution, and the fact that the 2D simulation cannot fully reproduce three-dimensional flow effects present in the experiments. Despite these minor discrepancies, the solver reliably reproduces the key trends in both surface pressure and skin friction for medium-strength SBLI cases. The heat flux also raised compared to 6° wedge case. This increase occurs because the stronger shock intensifies turbulence within the boundary layer and outer flow, while also compressing the flow near the wall, which raises both surface pressure and density. These combined effects enhance heat transfer to the wall, even in the separation region. As a result, the 10° wedge experiences higher peak heat fluxes compared to the 6° wedge case.

### *14° Shock generator case ( $\theta_w = 14°$)*

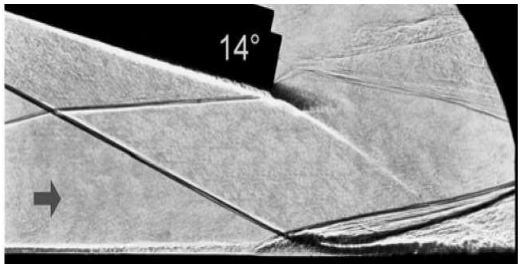


Fig. 25 Experimental shadowgraph for 14° wedge case

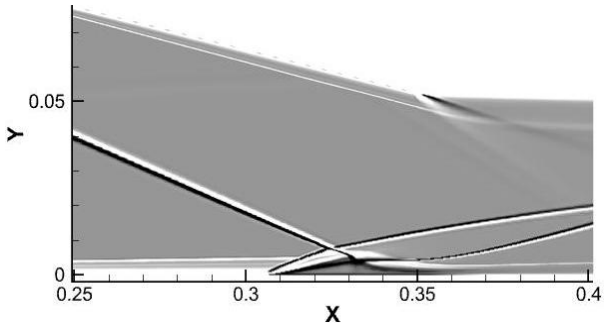


Fig. 26 Computational shadowgraph for 14° wedge case

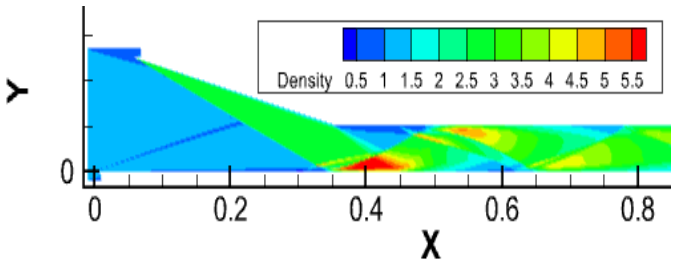


Fig. 27 Density contour for 14° wedge case

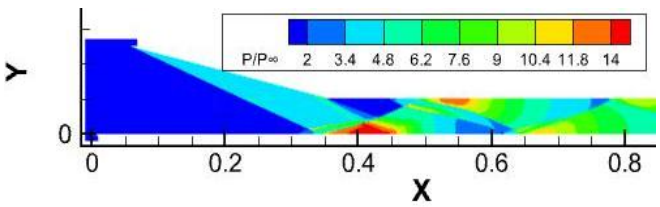


Fig. 28 Pressure contour for 14° wedge case

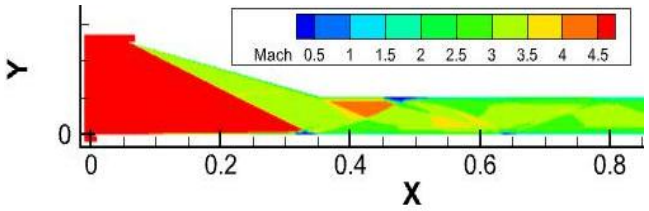


Fig. 29 Mach contour for 14° wedge case

For the 14° wedge case, a strong oblique shock is generated due to the higher flow deflection angle. When this shock impinges on the flat plate, it creates a strong adverse pressure gradient that the boundary layer cannot withstand, resulting in early and pronounced separation (see Fig. 25 and 26). Consequently, a large separation bubble forms, which is clearly visible in the pressure and velocity contours. Within this separated region, the flow decelerates significantly, and complex recirculation zones develop. Downstream of the separation bubble, the flow undergoes reattachment, accompanied by a strong reattachment shock. The interaction between the reattachment shock and the shear layer leads to high levels of turbulence, localized heating, and unsteady flow behaviour. In some regions, secondary separation zones or small vortices may form due to the highly disturbed flow structure. Overall, this case represents a strong shock-boundary layer interaction, where shock-induced separation dominates the flow behaviour, causing substantial pressure rise, large-scale unsteadiness, and significant loss in aerodynamic efficiency [9][13].

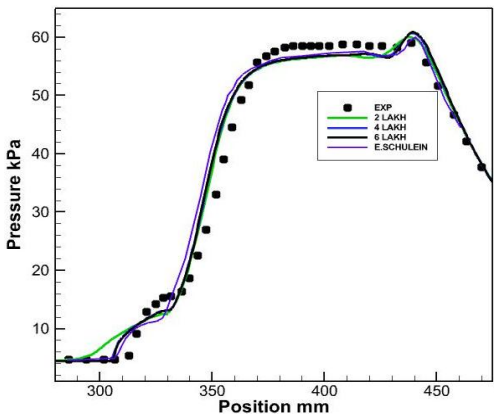


(a)

International Journal of Engineering Research & Technology (IJERT)
ISSN: 2278-0181
Vol. 15 Issue 04 , April - 2026

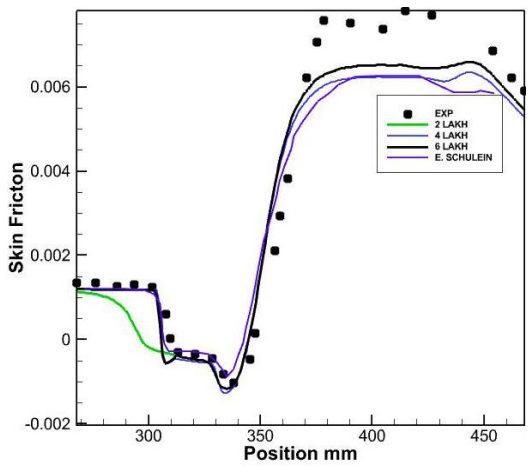


(b)

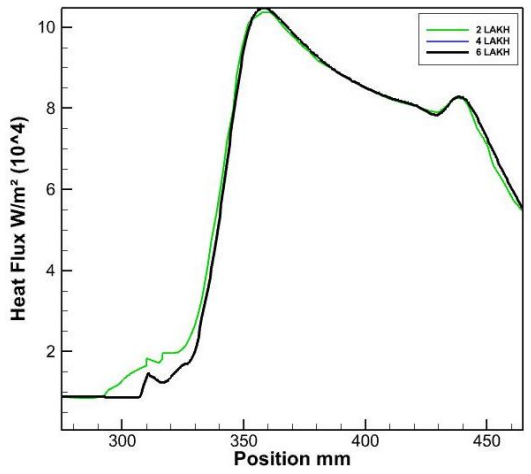


(c)

Fig. 30 (a) Surface pressure, (b) Skin Friction validation and (c) Heat Flux Distributions for 14° wedge case

A strong oblique shock from the 14° wedge causes a large surface pressure rise than 6 ° and 10 ° wedge cases. High pressure loads from this interaction can increase aerodynamic drag and impose additional structural stress. This pressure behavior confirms the 14° wedge case represents a strong shock boundary layer interaction, validating the need for detailed CFD and experimental comparison. The error percentage between SU2 and experimental pressure is approximately 0.79% (see Fig. 30 (a)).The skin friction coefficient is positive and relatively flat initially, indicating attached boundary layer with no major disturbances. Skin friction starts to decrease sharply and eventually drops to zero. This marks the point of boundary layer separation. $C_f$ becomes negative, indicating reversed flow in the separation bubble classic signature of a shock induced separation zone. $C_f$ rises sharply as the boundary layer reattaches. This rise reflects the reattachment shock and the acceleration of the flow back along the wall. Experimental $C_f$ continues to rise and peaks above 0.009, while SU2 levels of around 0.006. This under prediction suggests it struggles to fully capture the post reattachment shear layer development likely due to turbulence model limitations and mesh resolution (see Fig. 30 (b)). The wall heat flux for the 14° wedge case is higher than that for the 6° and 10° wedge case. This increase occurs because the stronger shock intensifies turbulence within the boundary layer and outer flow, while also compressing the flow near the wall, which raises both surface pressure and density. These combined effects enhance heat transfer to the wall, even in the separation region. Hence it is studied that the increasing wedge angles has also strengthened the oblique shock which has formed from the shock generator (wedge) and resulted in large amount of flow separation when compared to other two wedge angles.

## V. CONCLUSIONS

In this research effort, the laminar simulations computed for varied wedge angles revealed the effects of wedge angle, Reynolds number, and freestream conditions on shock boundary layer interactions. The 6° wedge produced only minor separation bubbles, whereas the 10° and 14° wedges generated stronger shocks and more pronounced separation. Reynolds number variations significantly influenced boundary layer behaviour: lower Reynolds numbers resulted in thicker, weaker boundary layers, causing earlier separation, deeper negative $C_f$ peaks, and shorter separation bubbles. Higher Reynolds numbers led to thinner, more energetic layers, reducing negative $C_f$ peaks but extending the separation length due to delayed reattachment. Freestream pressure variations also affected boundary layer properties and shock strength, demonstrating the coupled influence of viscous and inviscid effects on laminar SWBLI.

The RANS simulations using the SU2 solver were validated against experimental data for turbulent shock boundary layer interactions over 6°, 10°, and 14° wedges. For small wedge angles (6°), the separation bubble is minimal and has negligible impact on wall shear or aerodynamic loads. In contrast, larger wedge angles (10° and 14°) produce significant separation, affecting both skin friction and aerodynamic forces. The skin friction coefficient drops to zero and becomes negative in regions of flow reversal, consistent across all wedge angles. Pressure predictions show excellent agreement with experiments, with errors below 5%, while skin friction predictions exhibit larger deviations (>10%) due to turbulence modelling limitations and mesh resolution. Strong SWBLI increases wall shear stress and drag, highlighting its critical influence on hypersonic vehicle design and performance.

## REFERENCES

1. Touré, P.S.R. and Schülein, E., (2018). Numerical and experimental study of nominal 2-D shock-wave/turbulent boundary layer interactions. AIAA Paper 2018-3395. 2018 AIAA Fluid Dynamics Conference.
2. Hildebrand, N., Dwivedi, A., Nichols, J.W., Jovanović, M.R. and Candler, G.V., (2017). Simulation and stability analysis of oblique shock wave/boundary layer interactions at Mach 5.92. AIAA Journal, 55(10), pp.334 3364.
3. Willems, S., Gülhan, A., and Steelant, J., "Experiments on Shock-Induced Laminar-Turbulent Transition on a Flat

International Journal of Engineering Research & Technology (IJERT)
ISSN: 2278-0181
Vol. 15 Issue 04 , April - 2026

Plate at Mach 6," *Experiments in Fluids*, Vol. 56, No. 3, 2015, Article 49.

4. Deepak, N. R., Gai, S. L., and Neely, A. J., A computational investigation of laminar shock/wave boundary layer interactions, The Aeronautical Journal, 117(1187), 2013, pp. 27–56.
5. Babinsky, H., and Harvey, J. K., *Shock Wave-Boundary-Layer Interactions*, Vol. 32, Cambridge University Press, Cambridge, England, U.K., 2011.
6. Babinsky, H., and Harvey, J. K., *Shock Wave-Boundary-Layer Interactions*, Vol. 32, Cambridge University Press, Cambridge, England, U.K., 2011.
7. Touré, P. S., and Schülein, E., "Numerical and Experimental Study of Nominal 2-D Shock-Wave/Turbulent Boundary Layer Interactions," *2018 Fluid Dynamics Conference*, AIAA Paper 2018-3395, June 2018.
8. Baidya, R., Scharnowski, S., Bross, M., and Kähler, C., "Interactions Between a Shock and Turbulent Features in a Mach 2 Compressible Boundary Layer," *Journal of Fluid Mechanics*, Vol. 893, 2020
9. Zhang, D., Liu, W., Wang, B., and Su, Y., "Numerical Simulation on the Shock Wave/Boundary Layer Interaction with Heating/Cooling Effect," *Procedia Engineering*, Vol. 126, 2015, pp. 194–198.
10. D. Knight, H. Yan, A. G. Panaras, and A. Zheltovodov, "Advances in CFD prediction of shock wave turbulent boundary layer interactions," *Department of Mechanical and Aerospace Engineering, Rutger.The State University of New Jersey; Consulting Engineer, Athens, Greece; Institute of Theoretical and Applied Mechanics, Siberian Branch of the Russian Academy of Sciences*, Year.
11. Dolling, D. S., "Fifty Years of Shock-Wave/Boundary-Layer Interaction Research: What Next?" *AIAA Journal*, Vol. 39, No. 8, 2001, pp. 1517–1531.
12. Palacios, F., Alonso, J., Duraisamy, K., Colonno, M., Hicken, J., Aranake, A., Campos, A., Copeland, S., Economon, T., Lonkar, A., et al., "Stanford University Unstructured (SU2): An Open-Source Integrated Computational Environment for Multi-Physics Simulation and Design," *51st AIAA Aerospace Sciences Meeting Including the New Horizons Forum and Aerospace Exposition*, AIAA Paper 2013-0287, 2013.
13. Schülein, E., "Skin Friction and Heat Flux Measurements in Shock/Boundary Layer Interaction Flows," *AIAA Journal*, Vol. 44, No. 8, 2006, pp. 1732–1741